Nanoindentation differentiates tissue-scale functional properties of native articular cartilage

Cheng Li,[1] Lisa A. Pruitt,[1,2] Karen B. King[1,3]
[1]*UCB/UCSF Joint Graduate Group in Bioengineering, University of California, Berkeley, California*
[2]*Department of Mechanical Engineering, University of California, Berkeley, California*
[3]*Department of Medicine, University of California, San Francisco, California*

Received 25 August 2005; revised 17 December 2005; accepted 19 January 2006
Published online 31 May 2006 in Wiley InterScience (www.interscience.wiley.com). DOI: 10.1002/jbm.a.30751

Abstract: Cartilage mechanical properties are typically tested at the macroscale. To demonstrate the ability of nanoindentation to characterize *in situ* articular cartilage properties at the tissue scale, we investigated the local structure–property relationships of intact articular cartilage of a normal rabbit metacarpophalangeal joint. We calculated the mechanical parameters of stiffness, S, resistance to penetration, R, and volumetric creep strain, dV/V, from nanoindentation of the articular surface at specific regions of interest. We measured morphological parameters of superficial zone thickness, middle zone thickness, total uncalcified thickness, and cell density from corresponding regions with light and polarized light microscopy. Mechanical parameters were compared to morphological parameters. There were significant positive correlations ($r = 0.98$, $p < 0.05$) between superficial zone thickness and both S and R. However, we found no significant correlation between dV/V and the zone sizes. There were moderate, negative correlations between cell density and both S and R, suggesting an effect of cell volume on cartilage behavior at the tissue scale. We opine that the superficial zone plays important role in load support, as evidenced by correlations between zone size and intact cartilage mechanical properties. © 2006 Wiley Periodicals, Inc. J Biomed Mater Res 78A: 729–738, 2006

Key words: cartilage; microscale; microstructure; mechanics; nanoindentation

INTRODUCTION

Articular cartilage is a remarkable tissue in which heterogeneous composition and hierarchical structure provide optimized function in load support and joint lubrication.

Yet, due to the prevalence of articular cartilage ailments such as osteoarthritis and the poor intrinsic healing capacity of this tissue, there is a great demand for an articular cartilage substitute. The goal of tissue engineering repair strategies is to achieve structurally and functionally equivalent tissue to restore diseased or damaged cartilage.[1,2] Mechanical and morphological properties of native and engineered tissues are therefore important features to assess in determining functionality.

There are different scales of composition and organization in articular cartilage. This structural tissue consists primarily of water (60–85%), solid matrix consisting of collagen (15–22%) and proteoglycan (4–7%), and chondrocytes (3–5% of the tissue by volume), the cells which synthesize and maintain essential matrix molecules.[3] As an example of its structural complexity, articular cartilage can be divided into distinct zones according to collagen fiber organization and chondrocyte morphology through the thickness. Collagen fibers are arranged parallel and perpendicular to the articulating surface at the superficial and deep zones, respectively, and are randomly oriented in the middle zone. Chondrocytes in different zones also have characteristic morphology and different metabolic activities.[4]

The majority of studies measuring cartilage mechanical properties have tested excised tissue specimens at the macroscale. Such procedures typically involve confined or unconfined compression and simplified mechanics models.[5–8] A limitation of these methods is the requirement of punched tissue sam-

The contents of this publication are solely the responsibility of the authors and do not necessarily represent the official views of the CDC.

Correspondence to: K. B. King; e-mail: Karen.King@ucsf.edu

Contract grant sponsor: Centers for Disease Prevention and Control (CDC); contract grant number: R01 OH007786
Contract grant sponsor: Centers for Disease Control and Prevention (CDC); contract grant number: T42 CCT 910427

ples. Cutting the cartilage alters the collagen network structure and mechanical response of the tissue under loading. This alteration is undesired because an intact collagen matrix substantially constrains lateral displacement and helps to support load in the articular joint.[9,10] Furthermore, the determined bulk mechanical properties often do not address the nonlinear anisotropic and inhomogeneous nature of cartilage and are not representative of true tissue behavior. Moreover, bulk testing on tissue samples does not capture the local variations in tissue composition and organization which define microscale tissue properties.

To date, a few studies have demonstrated that the tissue mechanical properties are region- and depth-dependent in articular cartilage.[11–14] However, direct comparisons of local mechanical properties and morphological features of the same regions have not yet been made.

An alternative technique, nanoindentation, has the ability to localize mechanical properties on the micron to submicron lengths scales and at micrometer to nanometer depths. This technique has effectively characterized many materials, ranging from metallic and piezoelectric films[15,16] to mineralized tissues such as bone,[17] teeth,[18] and arterial calcifications.[19] More recently, nanoindentation was used to measure the mechanical properties of soft elastomeric materials such as poly(dimethyl siloxane),[20] and even hydrated materials such as agarose gel[21] and repair cartilage tissue.[22] Nanoindentation theory and instrumentation as applied to soft polymeric materials and biological tissues continue to be investigated.[20–23]

The local tissue properties measured by nanoindentation reflect the heterogeneous constituent composition and hierarchical organization in articular cartilage, rendering this technique an attractive tool for cartilage mechanics. The small size of the indenter tip allows high resolution *in situ* sampling of intact articular cartilage in small joints. Therefore, nanoindentation testing of cartilage confers minimal disruption of anatomy. In addition, the full range of tissue complexities is captured in the data analysis. Such characterization is useful for tissue engineering applications where knowledge of tissue-scale properties is a prerequisite for the design of engineered cartilage. The goals of the present study are to characterize *in situ* microscale articular cartilage properties of a normal rabbit metacarpophalangeal (MCP) joint and to examine the local structure–property relationships of intact articular cartilage. Given that articular cartilage is organized in the superficial, middle, and deep zones, which reflect the organization of the collagen network, and given that collagen is the major structural component of cartilage, our primary hypothesis is that the size of each specific cartilage zone affects the local mechanical properties of articular cartilage. On the contrary, despite the importance of chondrocytes within the tissue, their main function is metabolic. Therefore, our secondary hypothesis is that chondrocyte density does not affect the local mechanical properties of cartilage.

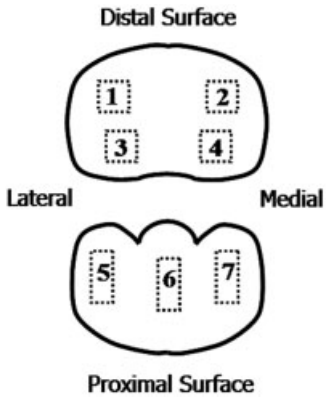

Figure 1. Schematic of the MCP joint of the left front paw. Seven ROI correspond to where mechanical and histological measurements are taken. Marked boxes indicate a square pattern of four indentations applied at each of the distal ROI or a linear pattern of three indentations applied to each of the proximal ROI. The diameter of each distal or proximal specimen is ~16 mm^2. Note that the figure is not drawn to scale.

MATERIALS AND METHODS

Sample preparation for nanoindentation

The left forelimb of a skeletally mature female New Zealand White (NZW) rabbit was removed after euthanasia and stored frozen at −20°C. Prior to dissection, the limb was thawed at 4°C overnight. The MCP joint of the 3rd digit was dissected from the rest of the limb 1 h prior to mechanical testing. The limb was skinned, the outer connective tissue was removed, and the joint opened. Carpal and phalange bones were cut near their proximal and distal ends, respectively. The long ends of the bones were embedded in poly(methyl methacrylate) in individual polymer wells mounted on 15-mm metal atomic force microscope discs. The typical size of the specimen was ~16 mm^2. The specimen was oriented such that the cartilage surface was parallel to the metal disc at the predetermined anatomical regions of interest (ROI). The seven ROI were chosen to sample the joint variation as shown in Figure 1.

With the aid of the dissecting microscope, temporary, small reflective markers were placed on the cartilage surface at the chosen ROI. The reflective markers were easily identified using the indenter optics. The coordinates of the center of each marker were recorded with the Triboscan Version 7.1 software (Hysitron, Minneapolis, MN) before the markers were flushed off with phosphate buffered saline (PBS). The positioning accuracy was calibrated using 5% agarose gel, and the accuracy was determined to be ~1 μm.[21]

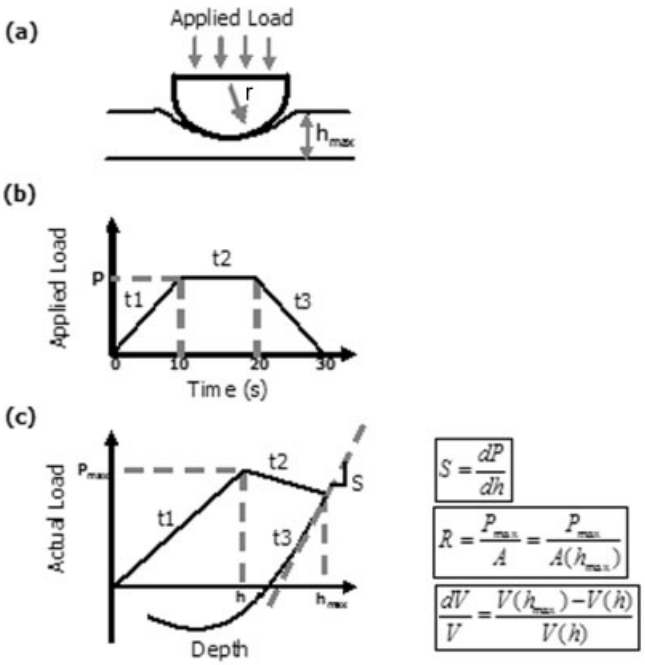

Figure 2. Nanoindentation data analysis schematic. (a) Cross sectional view of an indentation on sample, where r is the radius of the indenter tip (100 μm) and h_{max} is the maximum indentation depth. (b) Trapezoidal load profile as a function of time, where P is the maximum applied load (200 μN), t1 is the load segment, t2 is the hold segment, and t3 is the unload segment. Each segment is 10 s. (c) Load profile as a function of indentation depth, where P_{max} is the maximum load sensed by the sample, h is the depth at maximum load, and h_{max} is the maximum indentation depth. Equations for nanoindentation analysis are provided. Stiffness, S, is defined as the instantaneous slope of the unloading curve, where dP is the change in load and dh is the change in indentation depth over the 20–95% range of the load at initial unloading. Resistance to penetration, R, is defined as the maximum load over the area, where A is the contact area at maximum load. Volumetric creep strain, dV/V, is defined as the percent of displaced sample volume for the duration of the hold period, where V is the volume displaced during indentation.

Nanoindentation

All indentations were performed using the Hysitron TriboIndenter (Hysitron) with a 100 μm radius of curvature conospherical diamond probe tip [Fig.2(a)]. The round tip allowed for better conformity than a sharp tip during contact with the irregular and porous tissue surface. The chosen tip size was shown to best capture tissue-scale properties.[22]

Samples were kept hydrated in PBS throughout testing. A square pattern of four indentations was applied to each of the four distal ROI (sixteen total indentations). A linear pattern of three indentations was applied to each of the three proximal ROI (nine total indentations) (Fig. 1). The individual indentations were spaced 100 μm apart. For each indentation, the sample was loaded at the rate of 20 μN/s for 10 s, held at the maximum load of 200 μN for 10 s, and unloaded in the last 10 s [Fig. 2(b)]. Load–displacement data reflecting abrupt changes in force or displacement were discarded. The final data set contained two to three indentations for each ROI, from which mean and standard deviations of each ROI were calculated. The same indentations were then pooled correspondingly into the distal and proximal groups (ten and eight total indentations respectively) and averaged to produce the statistically acceptable estimates of the experimental value for the distal and proximal samples.

Nanoindentation data analysis

Mechanical properties calculated were stiffness (S), resistance to penetration (R), and volumetric creep strain (dV/V). These functional parameters, unlike the conventionally reported reduced modulus and hardness, do not require assuming a contact depth or area based on elastic theory.[24] The measured values capture an overall response of the material under the same set of loading conditions. Nanoindentation techniques were used to characterize cartilage repair tissues,[22] human arterial calcifications,[19] and dentin.[25–27]

In the present study, the initial unloading stiffness, shown schematically in Figure 2(c), was determined using Triboscan 7.1, according to the compliance method.[24] A power-law is fit to the unloading data and the stiffness, S, is defined as the first derivative of this curve at the maximum contact depth:

$$S = \frac{dP}{dh} \tag{1}$$

where dP is the change in load and dh is the change in displacement over a range of 20–95% of the load experienced at the initial unloading. The commonly reported reduced modulus is related to the stiffness as

$$E_r = \frac{S\sqrt{\pi}}{2\sqrt{A_c}} \tag{2}$$

where E_r is the reduced modulus and A_c is the theoretical projected contact area at the contact depth.[24] The reduced modulus is related to the Young's modulus through the equation

$$\frac{1}{E_r} = \frac{(1-v^2)}{E} + \frac{(1-v_i^2)}{E_i} \tag{3}$$

where E and ν are Young's modulus and Poisson's ratio for the specimen and E_i and ν_i are the same parameters for the indenter. Since in the present study, indication of adhesion between the tip and the sample[22] results in contact depths that are larger than predicted by elastic theory,[20] the alternative stiffness parameter is reported. This material stiffness parameter reflects a transitory elastic contact response under load.

Resistance to penetration can be interpreted as an equivalent measure of hardness. This parameter describes the material's ability to resist penetration by a surface contact for a given applied load and is expressed as

$$R = \frac{P_{max}}{A} = \frac{P_{max}}{A(h_{max})} \tag{4}$$

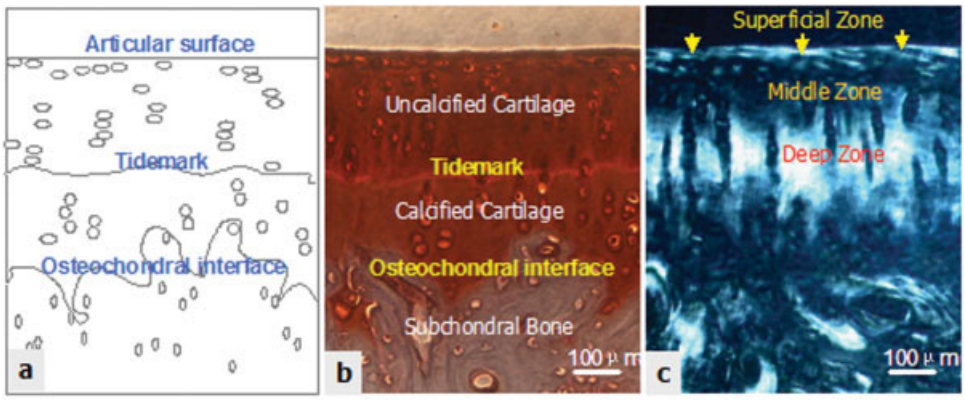

Figure 3. Illustrations showing cartilage zones through depth. (a) Schematic depicting three demarcations as seen in a typical photomicrograph. (b) Tissue section stained by safranin O and Hematoxylin. The uncalcified cartilage layer is distinguished from the calcified cartilage layer by the tidemark; the junction between cartilage and subchondral bone marks the osteochondral interface. (c) Photomicrograph of the serial section under polarized light. Bright regions represent the alignment of the collagen network fibers, as in the superficial and deep zones. Arrows point to the thin superficial zone. Dark or nonbirefringent regions represent the random collagen network organization of the middle zone. [Color figure can be viewed in the online issue, which is available at www.interscience.wiley.com.]

where P_{max} is the maximum load sensed by the sample, h_{max} is the displacement at P_{max}, and A is the projected area at this maximum load. Rather than the contact depth, the displacement at maximum load is used again because of the presence of adhesion, which would lead to contact depths and areas that are larger than predicted by elastic theory.[20] The indentation area is determined using the ideal area function for a spherical tip given by

$$A(h) = \pi h(2r - h) \tag{5}$$

where r is the radius of the indenter tip.

Lastly, the volumetric creep strain parameter quantifies the potential for recovery from tissue deformation. This parameter, described by the displaced volume during the hold period divided by the displaced volume at the beginning of the hold period, is expressed as

$$\frac{dV}{V} = \frac{V(h_{max}) - V(h)}{V(h)} \tag{6}$$

where h_{max} is the maximum displacement at the end of the hold period, and V is the displaced volume determined from the volume of a truncated sphere given by

$$V(y) = \left(\frac{\pi}{3}\right) y^2(3r - y) \tag{7}$$

where y is the displacement of the indenter tip or height of the truncated sphere.

Histology and morphological measurement

Following nanoindentation, the proximal and distal specimens were fixed in formalin for 24 h and decalcified in ethylene diaminetetraacetic acid (EDTA) for 2 weeks. The ROI of each specimen were then marked with green tissue ink (Cancer Diagnostics, Birmingham, MI) to aid in identification of the indentation position on histological sections. The specimens were dehydrated and treated in xylene substitute (Histoclear, National Diagnostics, Atlanta, GA) and processed for paraffin embedding. From each paraffin-tissue block, 6-μm thick sagittal sections with green ink marking were sectioned with a microtome and collected on glass slides. Each section contained cartilage zones from the joint surface through the subchondral bone (Fig. 3). Selected slides were used for light microscopy. Sections containing the ROI on these slides were stained with safranin O and Iron Hematoxylin and observed using the Axioskop 2 microscope (Carl Zeiss MicroImaging, Thornwood, NY). The remaining slides were dewaxed in xylene and sealed with a coverslip for observation of collagen network organization under polarized light.[28,29]

For each ROI, three to six quality tissue sections were averaged to give the morphological measurement representative of the ROI. For the proximal and distal samples, all the corresponding measurements (nine to fourteen sections) were averaged to give the statistically significant thickness and cell density measurements.

Light microscopy

Light microscopy was used to determine total uncalcified mean thickness and cell density. The reference point of each section was defined as the center of the green line atop the joint surface seen through the microscope objective. A photomicrograph was captured at 20× with the Carl Zeiss AxioCam using AxioVision 4.0 (Carl Zeiss MicroImaging). The same setting was used for all morphological measurements. Using the reference point as the midpoint, a width of 240 and 140 μm was defined for the ROI of the distal (square indentation pattern) and proximal (linear indentation pattern) samples, respectively (Fig. 1). These widths therefore corresponded to the total widths probed during nanoindentation experiments. Next, the contour of the uncalcified re-

gion was traced. This region spanned the width of the ROI and was bounded by the articular surface at the top and the tidemark at the bottom. The enclosed area of this uncalcified region was reported by AxioVision. The cells within the uncalcified region were manually counted and the cell density was calculated. The mean thickness was defined as the area of the region divided by the width. The mean uncalcified thickness and cell density were reported as two of the morphological parameters.

Polarized light microscopy

Polarized light microscopy was used to determine the superficial zone mean thickness and the middle zone mean thickness. Under polarized light, the green ink was not easily visualized. Therefore, light microscopy images with the reference points already marked were used to help locate the corresponding reference points on serial sections prepared for polarized light microscopy.

To maximize birefringence, the section was first rotated to 45° from the horizontal articular surface. Collagen fibers oriented either parallel or perpendicular to the primary axis of the joint appeared birefringent under polarized light. The superficial zone, with parallel fiber organization, was defined as a thin white band apparent at the surface of the tissue section. The middle zone was defined as the dark region flanked by the birefringent superficial and deep zones (Fig. 4).

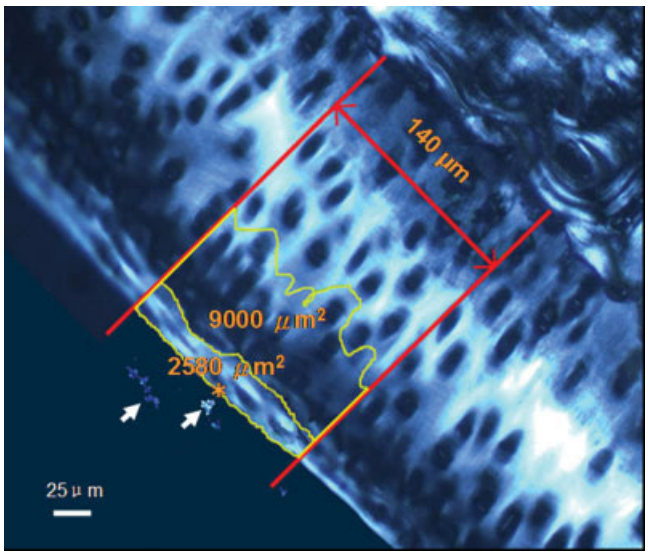

Figure 4. Illustration of area and mean thickness measurements on a photomicrograph of polarized light microscopy section of a distal ROI. Arrows point to speckles of the green ink at the joint surface. The asterisk (*) marks the reference point at the center of the green ink. A width of 140 μm is drawn with respect to the reference point to demarcate cartilage ROI from the joint surface through the subchondral bone. Bright regions represent alignment of the collagen network fibers, as in the superficial and deep zones. Dark regions represent the random collagen network organization of the middle zone. The superficial and middle zones are delineated by yellow lines with their respective area measurements. The mean thickness is defined as the zonal area divided by the width (140 μm in this case). [Color figure can be viewed in the online issue, which is available at www.interscience.wiley.com.]

TABLE I
Morphological Measurements for the Groups of Distal and Proximal Regions of Interest

	Distal	Proximal
Total uncalcified thickness (μm)	108.5 ± 36.2	138.5 ± 12.3
Superficial zone thickness (μm)	8.3 ± 1.6	13.4 ± 2.1
Middle zone thickness (μm)	51.0 ± 8.7	60.8 ± 8.2
Cell density (no. per mm^2)	1480 ± 607	1107 ± 388

Nine to fourteen sections of tissues were evaluated. Means ± SD are reported.

The superficial and middle zones were then outlined along their birefringent contours. The widths of the distal and proximal ROI were measured as above for the uncalcified region. The areas of the superficial and of the middle zones were recorded, and the superficial and middle zone mean thicknesses were calculated. Note that, for this study, the deep zone cartilage thickness was not determined because of the shallow depths of indentation into the tissue, approximately 1.2 μm.

Statistics

Analysis of variance was used to compare the morphological measurements and mechanical measurements between the different ROI, and the p values were determined using StatView Version 5.0.1 (SAS Institute, Cary, NC). Pearson's correlation test was fitted to each of the mechanical parameters—stiffness, resistance to penetration, and volumetric creep strain, *versus* morphological measurements—total uncalcified thickness, superficial zone thickness, middle zone thickness, and total uncalcified cell density. Pearson's correlation was also performed for pairs of the mechanical parameters. The correlation coefficients were calculated and evaluated for significance using a two-tailed unpaired student t-test ($\alpha = 5\%$, KaleidaGraph Version 3.5, Synergy Software, Reading, PA).

RESULTS

Tissue morphology

The mean and standard deviation of morphological measurements for the groups of distal and proximal ROI are shown in Table I. The average total uncalcified mean thickness, measured using light microscopy, ranged from 65.6 to 149.4 μm for the distal ROI and from 121.8 to 156.9 μm for proximal ROI. The average superficial zone mean thickness, measured using polarized light microscopy, ranged from 5.1 to 10.4 μm for distal ROI and from 10.4 to 18.5 μm for proximal

TABLE II
Mechanical Measurements for the Groups of Distal and Proximal Regions of Interest

	Distal	Proximal
Stiffness (N/m)	36.5 ± 27.4	146.9 ± 107.4
Resistance to Penetration (kPa)	31.5 ± 19.0	94.8 ± 45.2
Volumetric Creep Strain (%)	2.5 ± 0.8	16.9 ± 10.1

Means ± SD are reported.

ROI. The middle zone mean thickness, measured using polarized light microscopy, ranged from 37.4 to 68.6 μm for distal ROI and from 46.2 to 73.5 μm for proximal ROI. The proximal cartilage was thicker than the distal cartilage in the total uncalcified cartilage thickness ($p = 0.03$), superficial zone thickness ($p = 0.0001$), and middle zone thickness ($p = 0.007$). However, when considered as a fraction of the total uncalcified thickness, the zone thicknesses for the proximal and distal surfaces were comparable. The superficial zone thickness was ~8% of the total uncalcified thickness for the distal ROI and 10% for the proximal ROI. The middle zone thickness was ~50% for the distal ROI and 45% for the proximal ROI.

According to light microscopy, the distal ROI with cell density of 860–2600 cells/mm^2 was ~27% greater than the proximal ROI with 300–1700 cells/mm^2. However, the cell density difference between the proximal ROI and the distal ROI was not statistically significant.

Mechanical properties of intact tissue

The mean and standard deviation of mechanical measurements for the groups of distal and proximal ROI are shown in Table II. The stiffness, S, for the distal ROI ranged from 8.5 to 99.4 N/m and that for the proximal ROI ranged from 29.2 to 375.5 N/m. The resistance to penetration, R, for the distal ROI ranged from 8.2 to 75.0 kPa and that for the proximal ROI ranged from 36.1 to 157.2 kPa. The volumetric creep strain, dV/V, for the distal ROI ranged from 1.5 to 4.2% and that for the proximal ROI ranged from 4.5 to 36.8%. All three mechanical parameters had significantly greater values for the proximal data than the distal data, $p = 0.006$ for S, $p = 0.001$ for R, and $p = 0.0004$ for dV/V. The mean and standard deviation of the mechanical properties for the individual ROI are also reported in Table III. These data suggest high variability among ROI.

A positive correlation existed between any pair of the three mechanical parameters reported, both for the distal data, as shown in Figure 5(a–c), and for the proximal data, as shown in Figure 5(d–f). For the distal data, a strong and significant correlation existed between S and R ($p < 0.001$). However, the values for dV/V stayed relatively constant with increasing stiffness or resistance to penetration. For the proximal data, strong significant correlations existed between all pairs of the parameters: S correlated significantly with R ($p < 0.02$); R correlated significantly with dV/V ($p < 0.02$); and dV/V correlated significantly with S ($p < 0.001$).

Structure–property relationships

Pairs of morphological and mechanical measurements for the ROI were plotted as shown in Figures 6–9. No apparent correlations existed between the morphological and mechanical measurements for the proximal ROI. Therefore, correlation coefficients were determined for the distal data only. For the distal data, there were positive correlations between stiffness, S, and each of the zonal thicknesses (Fig. 6). However, the correlation was significant only between S and the superficial zone mean thickness ($p < 0.05$). Positive correlations existed between resistance to penetration, R, and each of the zonal mean thicknesses, as shown in Figure 7. Again, the correlation was significant only between R and the superficial zone mean thickness ($p < 0.05$). No significant correlations existed between the middle zone mean thickness and either S or R. Similarly, no significant correlation existed between the total uncalcified cartilage mean thickness and either S or R. Weak to moderate correlations existed between dV/V and each of the mean thicknesses (superficial zone, middle zone, and total uncalcified), as shown in Figure 8. However, none of the dV/V correlations was significant. Moderate negative correlations existed between cell density and the parameters S and R, as shown in Figure 9. However, dV/V weakly correlated with cell density. None of the cell density correlations was significant.

TABLE III
Mechanical Measurements for the Individual ROI

ROI	Stiffness (N/m)	Resistance to Penetration (kPa)	Volumetric Creep Strain (%)
Distal			
1	35.6 ± 23.2	34.3 ± 12.9	2.3 ± 0.5
2	57.7 ± 39.0	45.7 ± 26.5	2.6 ± 0.3
3	30.0 ± 4.0	25.2 ± 5.9	2.8 ± 1.9
4	12.8 ± 6.0	12.6 ± 6.2	2.2 ± 0.7
Proximal			
5	123.7 ± 68.5	112.8 ± 44.7	14.0 ± 8.1
6	86.1 ± 53.7	52.7 ± 17.6	12.2 ± 6.9
7	237.0 ± 145.0	131.0 ± 28.0	28.1 ± 12.3

Means ± SD are reported.

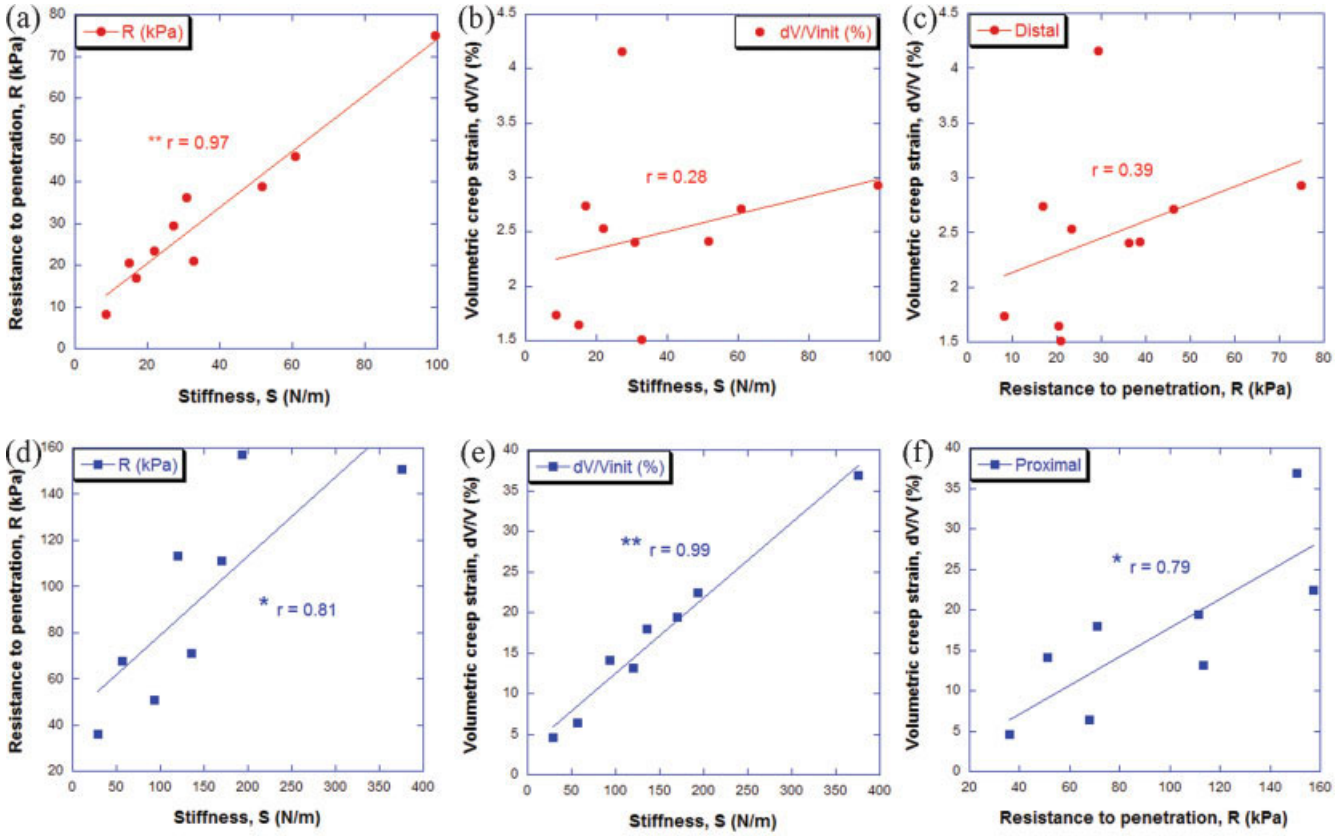

Figure 5. (a–c) are plots of correlations of mechanical properties for all distal data points (●); (d–f) are plots of correlations for all proximal data points (■). (a) shows the relationship between resistance to penetration, R, and stiffness, S, for the distal locations; (b) shows the relationship between volumetric creep strain, dV/V, and S for the distal locations; (c) shows the relationship between dV/V and R for the distal locations; (d) shows the relationship between R and S for the proximal locations; (e) shows the relationship between dV/V and S for the proximal locations; (f) shows the relationship between dV/V and R for the proximal locations. Pearson correlation coefficients (r) are reported. Significant correlations are indicated by (*) for $p < 0.02$ and (**) for $p < 0.001$. [Color figure can be viewed in the online issue, which is available at www.interscience.wiley.com.]

DISCUSSION

We demonstrate the ability of nanoindentation to differentiate functional properties of native articular cartilage at the tissue scale. Using nanoindentation techniques, we find that the superficial zone cartilage plays important role in load support, as evidenced by correlations between zone size and intact cartilage

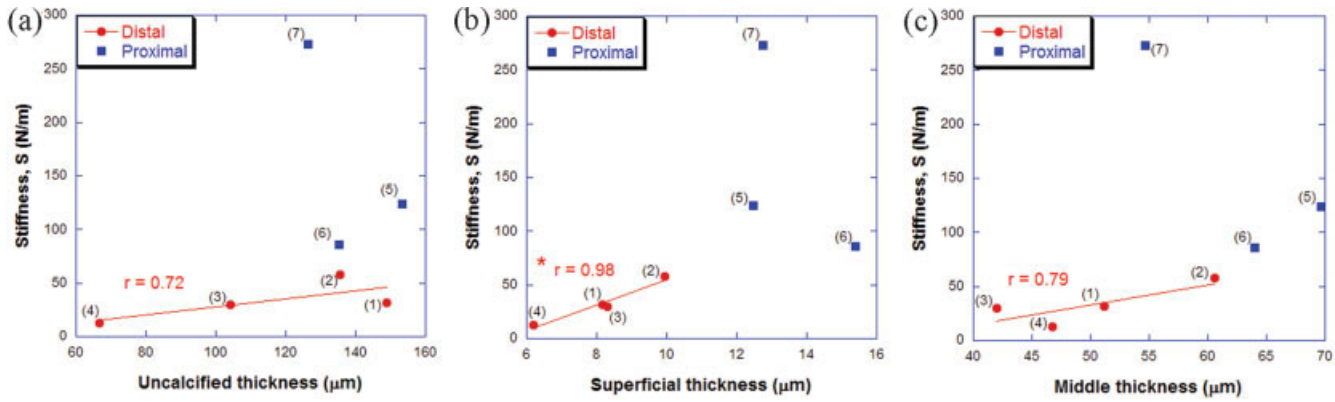

Figure 6. Plots of correlation between stiffness, S, and (a) uncalcified thickness, (b) superficial thickness, and (c) middle thickness for distal (●) and proximal (■) groups. Pearson correlation coefficients (r) are reported for distal data only. Data points are mean stiffness and thickness values. The ROI number is shown in parenthesis next to each data point. The correlation between S and superficial thickness (*) is significant ($p < 0.05$). [Color figure can be viewed in the online issue, which is available at www.interscience.wiley.com.]

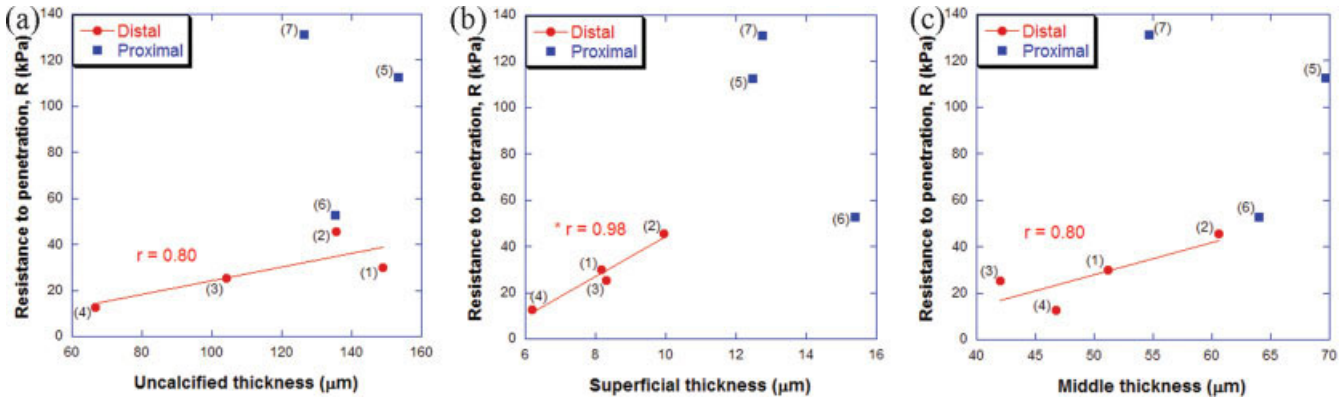

Figure 7. Plots of correlation between resistance to penetration, R, and (a) uncalcified thickness, (b) superficial thickness, and (c) middle thickness for distal (●) and proximal (■) groups. Pearson correlation coefficients (r) are reported for distal data only. Data points are mean resistance to penetration and thickness values. The ROI number is shown in parenthesis next to each data point. The correlation between R and superficial thickness (*) is significant ($p < 0.05$). [Color figure can be viewed in the online issue, which is available at www.interscience.wiley.com.]

mechanical properties. Furthermore, using the compliance method[24] and assuming the Poisson's ratio of cartilage to be $\nu = 0.3$,[3,12,30] the estimated Young's modulus for the ROI range from 0.5 ± 0.2 MPa to 2.2 ± 1.7 MPa for the distal surface and from 2.9 ± 1.9 MPa to 7.3 ± 5.7 MPa for the proximal surface. These values are on the same order of magnitude as compressive moduli reported in literature (about 1 MPa).[3]

The significant correlations between the superficial zone thickness and stiffness, S, and resistance to penetration, R, indicate the important role of distinct collagen network organization in providing tissue functions. In particular, the role of the well-known tangential alignment of the superficial collagen fibers in sustaining compressive loads through tensile stretching is pronounced at the tissue scale. This finding is consistent with bulk indentation characterization of the superficial zone cartilage.[11] As the superficial zone cartilage is essential for the maintenance of tissue properties[31,32], and is where fibrillation and fissure occur as a result of disease or cartilage damage, one would expect the superficial layer to be thicker, especially in high contact stress areas such as the convex ROI of the proximal articular surface.

Other studies show that mechanical properties of cartilage are dependent upon the topography of the articular surface. These studies indicate that different thicknesses develop at various regions in response to different loading states and functional demands of joint development.[33] Interestingly, although the absolute thickness measurements of the proximal surface are consistently greater than those of the distal surface in our findings, the percentages of total thickness for the individual zones are relatively constant for the proximal and distal surfaces. The superficial zone remains ~10% of the total uncalcified cartilage thickness across all ROI of both the proximal and distal articular surfaces. Clearly, the small fraction of the superficial

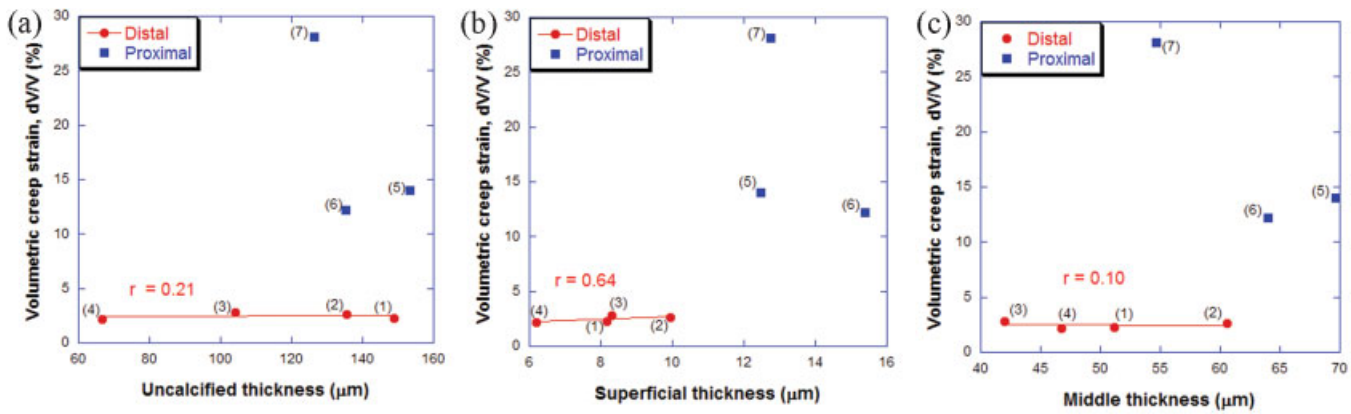

Figure 8. Plots of correlation between volumetric creep strain, dV/V, and (a) uncalcified thickness, (b) superficial thickness, and (c) middle thickness for distal (●) and proximal (■) groups. Pearson correlation coefficients (r) are reported for distal data only. Data points are mean volumetric creep strain and thickness values. The ROI number is shown in parenthesis next to each data point. [Color figure can be viewed in the online issue, which is available at www.interscience.wiley.com.]

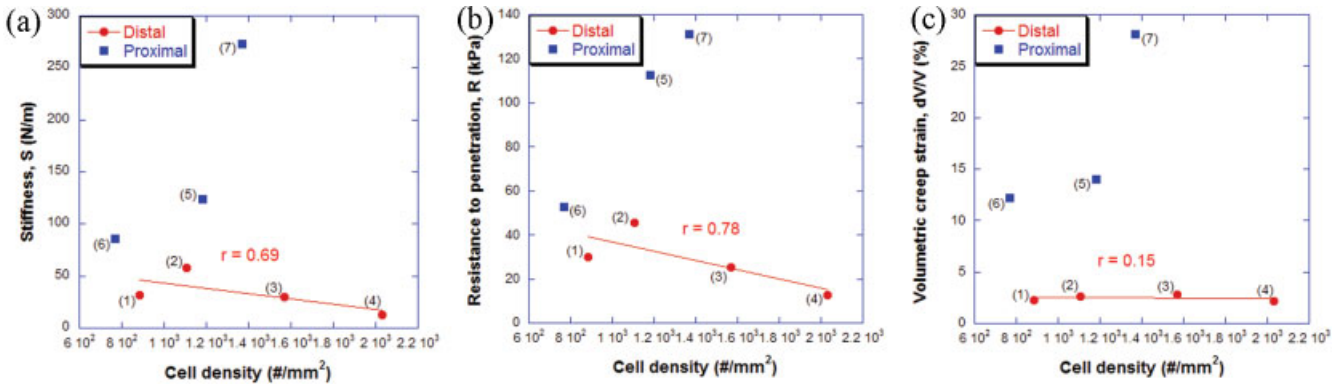

Figure 9. Plots of correlation between (a) stiffness, S, (b) resistance to penetration, R, and (c) volumetric creep strain, dV/V, and cell density for distal (●) and proximal (■) groups. Pearson correlation coefficients (r) are reported for distal data only. Data points are mean functional property and cell density values. The ROI number is shown in parenthesis next to each data point. [Color figure can be viewed in the online issue, which is available at www.interscience.wiley.com.]

cartilage layer is nontrivial. Moreover, the proximal and distal data display different strengths of correlations between the measured functional properties. This finding corroborates that the proximal and distal surfaces have fundamentally different functional requirements, as in part reflected by the difference in their tissue microstructural organization. However, the characteristic thinness of the superficial layer was reflected across all surface topographies sampled. Thus, it is speculated that stresses generated under loading are effectively transferred to the middle and deep zones. This enables each zone to contribute to the overall function of articular cartilage.

Furthermore, the mechanical parameters stiffness, S, and resistance to penetration, R, measured in the present study are reflective of normal joint cartilage function at the scale of the local collagen network structure. Both are expected to increase with increasing matrix volume (thickness). This is validated by significant positive correlations between S and R for both the distal and proximal data. The zone size and mechanical property findings in the present study highlight the distinct functional role the superficial zone assumes in the tissue.

A limitation of this work is that the nanoindentation method is a surface characterization technique. In this study, the low effective loads (less than 80 μN or 40% of the maximum applied force) and shallow depths (~1.2 μm or less than 20% of the thickness measurements) in testing cause the mechanical properties to be more reflective of the superficial zone rather than the deeper zones. This may account for the nonsignificant correlations involving middle zone and total uncalcified thicknesses.

The viscoelastic properties of cartilage arise from the time-dependent reorganization of the collagen matrix and the fluid exudation through the solid collagen-proteoglycan matrix.[3] The latter is believed to play a dominant role in the viscoelastic response because of the large quantity of water in the tissue.[3] The volumetric creep strain reflects the stress relaxation of the cartilage. This phenomenon is more prevalent in the middle and deep zones. The testing protocol employed in this study, however, is restricted predominantly to the superficial layer. The relatively constant values of volumetric creep strain suggest that the testing protocol is insensitive to the middle and deep layers. This is a likely explanation for the lack of correlation between volumetric creep strain and morphological parameters.

In this work, we find that the mechanical properties of the proximal surfaces are significantly greater than the distal surface. However, it should be noted that the standard deviations are large, particularly for stiffness. The standard deviation reflects variations in surface topography and variations in tissue properties within and amongst ROI. It is unclear at this time which of these factors is predominant, since there are no other published data on the local variations of cartilage property at the tens of micrometer length scale.

Another interesting finding of the present study is that cell density does not significantly correlate with cartilage mechanical parameters. This is reasonable, considering that cells consist of only a very small volume (3–5%) of the tissue, and the function of the chondrocytes is to maintain and remodel the matrix,[3] and not to support mechanical load. The negative correlation trends between cell density and stiffness and between cell density and resistance to penetration may indicate that the influence of the chondrocytes and their pericellular matrix, competing in tissue volume with the extracellular matrix, become relevant at the micron to tens of micron level.

In conclusion, we demonstrate measurements of cartilage mechanical properties at very small length scales (tens of micrometers). We find that superficial zone structure correlates to these properties. For fur-

ther insight on tissue-scale structure–property relationships, future studies will investigate the correlation of stiffness, resistance to penetration, and volumetric creep strain to more detailed microstructural features such as the distribution and organization of chondrocytes within the matrix and the concentrations of collagen and of proteoglycan. Using the experimental protocols piloted in this study, future studies will also test these structure and property findings in multiple animals.

We thank Song Seto, Laura Huang, and Howard Lan for assisting with sample preparation, histology, and microscopy protocol development.

References

1. Ateshian GA, Hung CT. Patellofemoral joint biomechanics and tissue engineering. Clin Orthop Relat Res 2005;436:81–90.
2. Guilak F, Butler DL, Goldstein SA. Functional tissue engineering: The role of biomechanics in articular cartilage repair. Clin Orthop Relat Res 2001;391 (Suppl):S295–S305.
3. Mow VC, Ratcliffe A, Poole AR. Cartilage and diarthrodial joints as paradigms for hierarchical materials and structures. Biomaterials 1992;13:67–97.
4. Kuettner KE, Schleyerbach R, Hascall VC. Articular Cartilage Biochemistry. New York: Raven Press; 1986. 456 p.
5. Mow VC, Kuei SC, Lai WM, Armstrong CG. Biphasic creep and stress relaxation of articular cartilage in compression? Theory and experiments. J Biomech Eng 1980;102:73–84.
6. Hayes WC, Herrmann G, Mockros LF, Keer LM. Mathematical-analysis for indentation tests of articular-cartilage. J Biomech 1972;5:541–551.
7. Li LP, Herzog W. Strain-rate dependence of cartilage stiffness in unconfined compression: The role of fibril reinforcement versus tissue volume change in fluid pressurization. J Biomech 2004;37:375–382.
8. Lai WM, Mow VC, Roth V. Effects of nonlinear strain-dependent permeability and rate of compression on the stress behavior of articular cartilage. J Biomech Eng 1981;103:61–66.
9. Soltz MA, Ateshian GA. A conewise linear elasticity mixture model for the analysis of tension-compression nonlinearity in articular cartilage. J Biomech Eng 2000;122:576–586.
10. Soulhat J, Buschmann MD, Shirazi-Adl A. A fibril-network-reinforced biphasic model of cartilage in unconfined compression. J Biomech Eng 1999;121:340–347.
11. Schinagl RM, Gurskis D, Chen AC, Sah RL. Depth-dependent confined compression modulus of full-thickness bovine articular cartilage. J Orthop Res 1997;15:499–506.
12. Laasanen MS, Saarakkala S, Toyras J, Hirvonen J, Rieppo J, Korhonen RK, Jurvelin JS. Ultrasound indentation of bovine knee articular cartilage in situ. J Biomech 2003;36:1259–1267.
13. Huang CY, Stankiewicz A, Ateshian GA, Mow VC. Anisotropy, inhomogeneity, and tension-compression nonlinearity of human glenohumeral cartilage in finite deformation. J Biomech 2005;38:799–809.
14. Tomkoria S, Patel RV, Mao JJ. Heterogeneous nanomechanical properties of superficial and zonal regions of articular cartilage of the rabbit proximal radius condyle by atomic force microscopy. Med Eng Phys 2004;26:815–822.
15. Zhou Y, Yang CS, Chen GF, Ding W, Ding L, Wang MJ, Wang YM, Zhang T, Zhang H. Measurement of Young's modulus and residual stress of copper film electroplated on silicon wafer. Thin Solid Films 2004;460:175–180.
16. Delobelle P. True Young modulus of Pb(Zr,Ti)O-3 films measured by nanoindentation. Appl Phys Lett 2004;85:5185.
17. Rho JY, Zioupos P, Currey JD, Pharr GM. Microstructural elasticity and regional heterogeneity in human femoral bone of various ages examined by nano-indentation. J Biomech 2002; 35:189–198.
18. Habelitz S, Marshall SJ, Marshall GW Jr, Balooch M. Mechanical properties of human dental enamel on the nanometre scale. Arch Oral Biol 2001;46:173–183.
19. Pruitt LA, Coughlin D. Nanoindentation of calcification from atherosclerotic carotid arteries. In: Transactions of the 7th World Biomaterials Congress. Sydney, Australia, May 17–21, 2004.
20. Carrillo F, Gupta S, Balooch M, Marshall SJ, Marshall GW, Pruitt L, Puttlitz CM. Nanoindentation of polydimethylsiloxane elastomers: Effect of crosslinking, work of adhesion, and fluid environment on elastic modulus. J Mater Res 2005;20: 2820–2830.
21. Ebenstein DM, Pruitt LA. Nanoindentation of soft hydrated materials for application to vascular tissues. J Biomed Mater Res A 2004;69:222–232.
22. Ebenstein DM, Kuo A, Rodrigo JJ, Reddi AH, Ries M, Pruitt L. A nanoindentation technique for functional evaluation of cartilage repair tissue. J Mater Res 2004;19:273–281.
23. Gupta S, Carrillo F, Li C, Pruitt LS, Puttlitz CM. Adhesive forces significantly affect elastic modulus determination of soft polymeric materials in nanoindentation. Materials Letters; in press.
24. Oliver W, Pharr G. An improved technique for determining hardness and elastic modulus using load and displacement sensing indentation experiments. J Mater Res 1992;7:1564–1583.
25. Kinney JH, Balooch M, Marshall SJ, Marshall GW Jr, Weihs TP. Atomic force microscope measurements of the hardness and elasticity of peritubular and intertubular human dentin. J Biomech Eng 1996;118:133–135.
26. Hosoya Y, Marshall GW Jr. The nano-hardness and elastic modulus of carious and sound primary canine dentin. Oper Dent 2004;29:142–149.
27. Hosoya Y, Marshall GW, Marshall GW Jr, Kinney JH, Balooch M, Marshall SJ, Weihs TP. The nano-hardness and elastic modulus of sound deciduous canine dentin and young premolar dentin—Preliminary study. J Mater Sci Mater Med 2005;16:1–8.
28. Kiraly K, Hyttinen MM, Parkkinen JJ, Arokoski JA, Lapvetelainen T, Torronen K, Kiviranta I, Helminen HJ. Articular cartilage collagen birefringence is altered concurrent with changes in proteoglycan synthesis during dynamic in vitro loading. Anat Rec 1998;251:28–36.
29. Williams JM, Uebelhart D, Thonar EJ, Kocsis K, Modis L. Alteration and recovery of the spatial orientation of the collagen network of articular cartilage in adolescent rabbits following intra-articular chymopapain injection. Connect Tissue Res 1996;34:105–117.
30. Roemhildt ML, Coughlin KM, Peura GD, Fleming BC, Beynnon BD. Material properties of articular cartilage in the rabbit tibial plateau. J Biomech; in press.
31. Guilak F, Ratcliffe A, Lane N, Rosenwasser MP, Mow VC. Mechanical and biochemical changes in the superficial zone of articular cartilage in canine experimental osteoarthritis. J Orthop Res 1994;12:474–484.
32. Setton LA, Zhu W, Mow VC. The biphasic poroviscoelastic behavior of articular cartilage: Role of the surface zone in governing the compressive behavior. J Biomech 1993;26:581–592.
33. Carter DR, Beaupre D, Beaupre G. Skeletal Function and Form: Mechanobiology of Skeletal Development, Aging, and Regeneration. Cambridge: Cambridge University Press; 2001.